Journal of Solid State Chemistry **168,** 275–283 (2002)
doi:10.1006/jssc.2002.9722

Order–Disorder Enhanced Oxygen Conductivity and Electron Transport in Ruddlesden–Popper Ferrite-Titanate $Sr_3Fe_{2-x}Ti_xO_{6+\delta}$

Y. A. Shilova,* M. V. Patrakeev,* E. B. Mitberg,* I. A. Leonidov,* V. L. Kozhevnikov,*,[1] and K. R. Poeppelmeier†

*Institute of Solid State Chemistry, Ural Division of RAS, Pervomaiskaia 91, GSP-145, Ekaterinburg 620219, Russia; and †Department of Chemistry, Northwestern University, 2145 Sheridan Road, Evanston, Illinois 60208

Received April 22, 2002; in revised form July 8, 2002; accepted July 16, 2002

The Ruddlesden–Popper ferrite $Sr_3Fe_2O_{6+\delta}$ and its titania-doped derivatives $Sr_3Fe_{2-x}Ti_xO_{6+\delta}$, where $0<x\leq 2$, have been characterized by X-ray powder diffraction and thermogravimetry. The changes in oxygen content and crystal lattice parameters are consistent with titanium ions entering the solid solution in 4+ oxidation state with octahedral oxygen coordination. Electronic conductivity measurements on polycrystalline $Sr_3Fe_2O_{6+\delta}$ and $Sr_3Fe_{0.8}Ti_{1.2}O_{6+\delta}$ in the temperature range 750–1000°C and oxygen partial pressures (pO_2) varying between 10^{-20} and 0.5 atm revealed that the predominant partial conductivity of electrons is proportional to $pO_2^{-1/4}$ in the low pO_2 region, while the predominant partial contribution of holes to the conductivity is proportional to $pO_2^{+1/4}$ in the high pO_2 range. The pressure-independent oxygen ion conductivity is found to decrease with the increase in titanium content. A possible pathway for oxygen ion migration is discussed in relation to disorder in the oxygen sublattice and titanium doping. © 2002 Elsevier Science (USA)

Key Words: **Ruddlesden–Popper ferrite; oxygen conductivity; oxygen transfer; electron conductivity; thermopower.**

INTRODUCTION

The oxygen vacancy ordering that often occurs in oxides is generally regarded as unfavorable for fast oxygen ion transport. In particular, this negative effect is well known for perovskites (1). On the other hand, significant oxygen ion conductivity, which follows from the high oxygen permeation fluxes reported, was reported recently in the solid solution $La_{1-x}Sr_xFe_{1-y}Ga_yO_{3-\delta}$ ($x = 0.1-0.4$; $y = 0.2 - 0.5$) claimed to have an oxygen vacancy ordered brownmillerite structure (2). Also, recent *in situ* high-temperature conductivity measurements corroborate that the ion conductivity can approach 0.1 S/cm at 900°C in the brownmillerite-like ferrite $Sr_2Fe_2O_{5+\delta}$ (3). To understand in more detail the influence structural vacancies have on transport, we have selected the Ruddlesden–Popper (RP) ferrite $Sr_3Fe_2O_{6+\delta}$ (4). This ferrite is characterized by the presence of oxygen-deficient double-perovskite layers $Sr_2Fe_2O_{5+\delta}$ sandwiched between SrO rock-salt layers (Fig. 1). Because the structure is stable with respect to changes of temperature and oxygen partial pressure over wide limits, and the occupancy of the O(3) site can vary depending on environmental parameters (5), titanium doping according to the formula $Sr_3Fe_{2-x}Ti_xO_{6+\delta}$ is an effective method to alter the oxygen population in the structural vacancies and, thus, to track respective changes in transport properties. These changes, monitored using the measurement of electrical conductivity in the temperature range 750–1000°C and oxygen pressure varying between 10^{-20} and 0.5 atm, were used to separate the different contributions to the conductivity and to determine the main parameters governing transport of oxygen ions and electrons.

EXPERIMENTAL

The samples used in this study were prepared by a conventional solid-state reaction method. Starting materials were oxides Fe_2O_3 (99.2%), TiO_2 (99.5%) and strontium carbonate $SrCO_3$ (99.94%). The raw materials were pre-calcined to remove adsorbates, weighed in desirable amounts and thoroughly mixed with a mortar and pestle with the addition of ethanol. The mixtures were pressed into pellets by a mechanical pressing technique and fired at 900–1300°C in air. The materials were crushed into powder, pressed and fired several times with a gradual increase in temperature before single-phase specimens were obtained. The phase purity control and determination of crystal lattice parameters were carried out using X-ray diffraction (XRD) ($\lambda = 1.54178$ Å). The reduction

[1] To whom the correspondence should be addressed: Fax: +7-3432-74-00-03. E-mail: kozhevnikov@imp.uran.ru.

0022-4596/02 $35.00

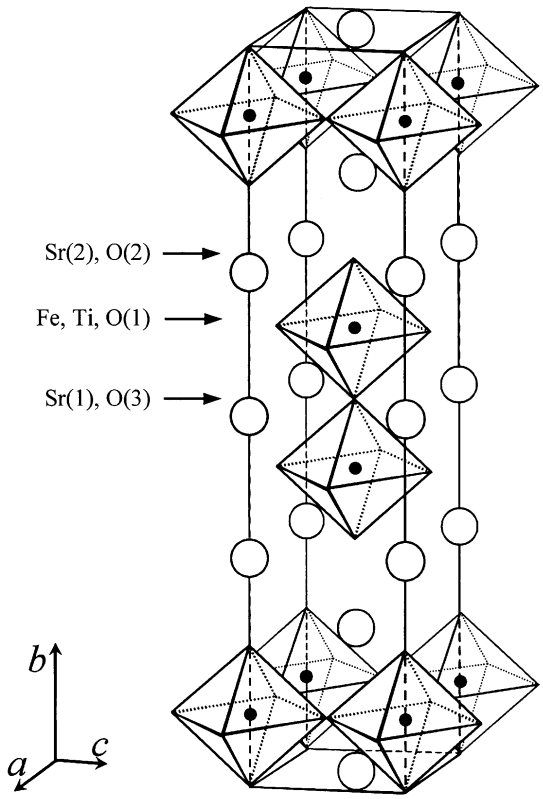

FIG. 1. A sketch of the elementary unit of the Ruddlesden–Popper ferrite $Sr_3Fe_2O_{6+\delta}$. Strontium and iron/titanium cations are shown with empty and filled circles, respectively. Oxygen coordination of iron/titanium cations is shown with octahedra. Oxygen structural vacancies reside in O(3) positions.

experiments and studies of oxygen content changes in the specimens as a function of temperatures were carried out with a Setaram TG-DTA-92 thermoanalyzer. Also, a vertical tubular furnace was used for high-temperature treatments of specimens in different atmospheres. When necessary, quenching was performed by dropping samples into a crucible with liquid gallium that rested in the lower end of the tubular compartment at room temperature. The independent determination of oxygen content in as-prepared samples was carried out using iodometric titration as described previously (6).

Powders of $Sr_3Fe_2O_{6+\delta}$ and $Sr_3Fe_{0.8}Ti_{1.2}O_{6+\delta}$ were pressed into disks under 2 kbar uniaxial load. The disks were sintered at 1350°C to a density of about 92% of the theoretical. Rectangular bars $2 \times 2 \times 18$ mm were cut from the sintered disks for the four-probe d.c. conductivity measurements. The current leads and voltage probes were made of platinum wire (with diameter of 0.3 mm) and tightly wound to the specimen with 12 and 8 mm spacing, respectively. Platinum metal is known as a reversible oxygen gas electrode. Therefore, the measured conductivity may include a contribution from oxygen ions. The measurements were carried out in a cell utilizing the oxygen sensing and pumping properties of zirconia as described elsewhere (7). The cell was filled with a gas mixture containing 50% O_2:50% CO_2 and sealed. The electrical parameters were measured with a high-precision voltmeter Solartron 7081. Computer-controlled operation of the oxygen pump and sensor provided precise variation and maintenance of the partial oxygen pressure in the cell. The measurements were carried out in the mode of decreasing oxygen partial pressure in isothermal runs. Individual data points were recorded upon achievement of equilibrium between the sample and ambient atmosphere. The criterion for achieving equilibrium was a relaxation rate less than 0.01% per minute in the logarithm of the conductivity under a fixed oxygen pressure inside the cell. The time to achieve equilibrium after a change in the oxygen pressure over a sample varied and was dependent on temperature, oxygen partial pressure and cation composition. The measurements were halted upon achievement of the desirable low-pressure limit. Then the oxygen pressure was increased to the starting upper limit where measurements were repeated in order to confirm reversibility of the experiment; thereupon temperature was changed thus enabling the next measuring cycle.

RESULTS

The X-ray patterns of the specimens $Sr_3Fe_{2-x}Ti_xO_{6+\delta}$ slowly cooled in air show formation of the tetragonal solid solution within the entire range $0 \le x \le 2$. The elementary unit parameters in the as-prepared $Sr_3Fe_2O_{6+\delta}$ agree with a previous report (5) and are shown in Fig. 2 together with the results for titanium-substituted samples. The increase in the lattice parameters with the substitution level is consistent with replacement of iron cations (3+ and 4+ oxidation states; $r_{VI}(Fe^{3+}) = 0.58$ Å, $r_{VI}(Fe^{4+}) = 0.585$Å)

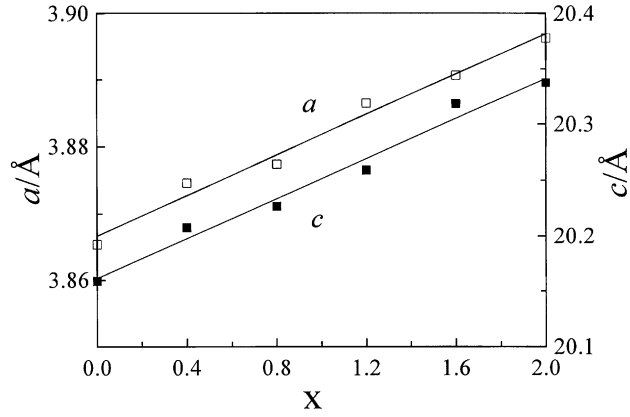

FIG. 2. The elementary unit parameters versus titanium doping in as-prepared $Sr_3Fe_{2-x}Ti_xO_{6+\delta}$.

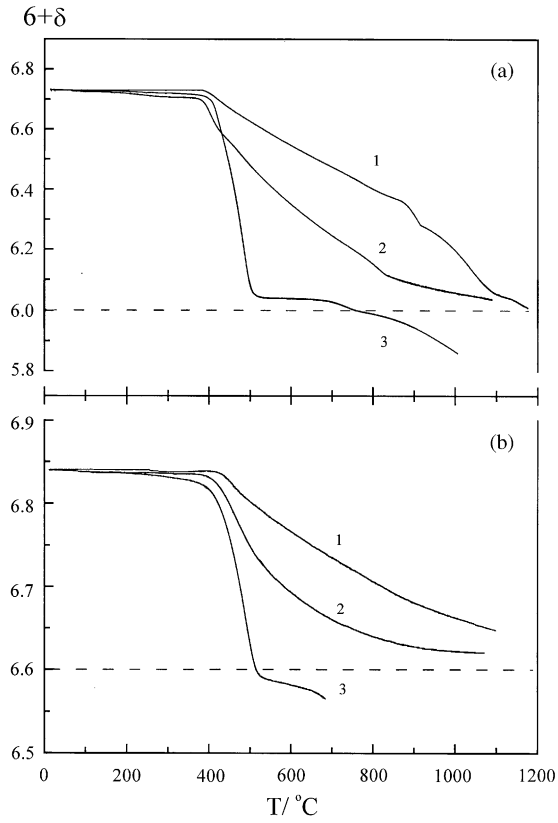

FIG. 3. The oxygen content change in $Sr_3Fe_2O_{6+\delta}$ (a) and $Sr_3Fe_{0.8}Ti_{1.2}O_{6+\delta}$ (b) at heating in air (1), helium (2) and gas mixture 5% H_2:95% He (3).

(8)) with larger titanium cations (4+ oxidation state; $r_{VI}(Ti^{4+}) = 0.605$ Å) (8)). The oxygen content of the as-prepared oxide $Sr_3Fe_2O_{6+\delta}$ is found equal to $6+\delta = 6.73$, which again is in close correspondence with $6+\delta = 6.74$ observed before (5). Hence, the electrical neutrality of the crystalline lattice results in Fe^{3+} and Fe^{4+} cations coexisting in the oxide, which is represented by the formula $Sr_3Fe^{3+}_{0.54}Fe^{4+}_{1.46}O_{6.73}$. Heating in air ($pO_2 = 0.21$ atm) or in helium ($pO_2 \approx 10^{-3}$ atm) results in the depletion of oxygen from the sample and gradual reduction of the Fe^{4+} cations, (Fig. 3a). At temperatures above 1000°C, the oxygen content approaches $6+\delta = 6.0$ consistent with the formula $Sr_3Fe^{3+}_2O_6$. The XRD pattern of the specimen fired at 900°C in the atmosphere containing 5% of hydrogen and 95% of helium did not reveal phases other than the initial strontium ferrite. It can be seen from the respective thermogravimetry (TG) plot in (Fig. 3a) that the total oxygen content $6+\delta$ in the ferrite $Sr_3Fe_2O_{6+\delta}$ can achieve values less than 6. In other words, heating in a strongly reducing atmosphere results in the complete exhaustion of oxygen from O(3) positions and the formation of oxygen vacancies in other oxygen positions. The most probable site for the formation of these extra vacancies is the O(1) position. Vacancies in the apical O(2) position would result in energetically unfavorable square-planar coordination of iron cations. The thermal behavior of the substituted specimens is quite similar; however, the oxygen homogeneous range becomes smaller with the increase in the substitution level. For example, TG curves for $Sr_3Fe_{0.8}Ti_{1.2}O_{6+\delta}$ are shown in (Fig. 3b). The oxygen content of the as-prepared specimen was found to be equal to 6.84. Assuming a 4+ oxidation state for the titanium cations, the formula can be represented as $Sr_3Fe^{3+}_{0.32}Fe^{4+}_{0.48}Ti^{4+}_{1.2}O_{6.84}$. Figure 3b demonstrates that the total amount of oxygen, which can reversibly be removed from the oxide, is close to 0.24. The XRD pattern of the sample fired at 650°C in the atmosphere 5% H_2:95% He did not reveal impurity phases. From the respective TG plot, Fig. 3b, one can see that the total oxygen content in $Sr_3Fe_{0.8}Ti_{1.2}O_{6+\delta}$ can achieve values smaller than 6.6 under strongly reducing conditions. Based on the TG results, variations in the oxygen content and in the amount of Fe^{3+} and Fe^{4+} cations with titanium substitution can be rationalized with the formula $Sr_3Fe^{3+}_{2-x-2\delta}Fe^{4+}_{2\delta}Ti^{4+}_xO_{6+x/2+\delta}$. That is to say, substitution of iron with titanium results in proportional and practically irreversible filling of the vacancies in the O(3) site, and although the total amount of oxygen in the as-prepared oxide $(6+x/2+\delta)$ increases with x, the amount δ of the labile oxygen becomes smaller, thus reflecting a decrease in the number of O(3) positions available for oxygen exchange. The complete exhaustion of the labile oxygen from O(3) positions results in the formation of the oxide $Sr_3Fe^{3+}_{2-x}Ti^{4+}_xO_{6+x/2}$ containing iron cations in 3+ oxidation state only. In a practical sense, the crystalline state of the oxide tolerates a small amount of oxygen vacancies, most likely in the O(1) position. Such an oxygen-deficient state corresponds to the coexistence of Fe^{2+} and Fe^{3+} cations or $Sr_3Fe^{2+}_{2\delta}Fe^{3+}_{2-x-2\delta}Ti^{4+}_xO_{6+x/2-\delta}$.

The conductivity curves obtained for specimens with $x = 0$ and 1.2 are shown in Fig. 4. It follows from the data that both parent and substituted ferrites are stable (single phase) to about $pO_2 = 10^{-20}$ and 10^{-16} atm at 750°C and 1000°C, respectively. These data also show (Fig. 4) that titanium doping results in a decrease of the total conductivity. The conductivity variations with oxygen partial pressure are nearly proportional to $pO_2^{+1/4}$ at $pO_2 > 10^{-5}$ atm. At smaller pressures of oxygen, nearly flat portions on the conductivity isotherms appear, where the change in conductivity is relatively small with oxygen pressure variations. These portions cover larger spans of the oxygen pressure when the temperature decreases. It is important to notice that the conductivity equilibration kinetics are very sluggish in these pressure intervals, which is evidenced by the much longer time (several hundred hours) required to attain equilibrium. As a consequence, the conductivity data, which were obtained at these

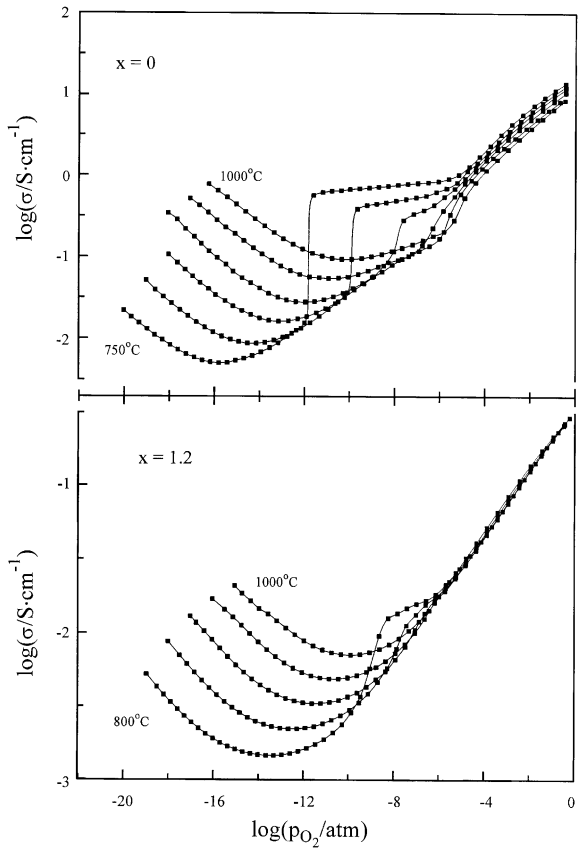

FIG. 4. The measured conductivity isotherms in $Sr_3Fe_{2-x}Ti_xO_{6+\delta}$ ($x = 0$ and 1.2) versus the logarithm of the oxygen partial pressure. Solid lines serve as a guide to the eye.

pressures under the equilibrium criterion described earlier, may not correspond perfectly to equilibrium values. Further decrease in the pressure results in a step-like drop of the conductivity, whereupon the equilibration time reverts to more reasonable values (dozens of hours). The conductivity continues to decrease with the pressure and is nearly proportional to $pO_2^{+1/4}$, achieves a minimal value, and then begins to increase where it is nearly proportional to $pO_2^{-1/4}$. The sharp changes in the shape of the isotherms in the middle-pressure range are not related to changes in the crystalline structure, as evidenced by the XRD patterns of the specimens fired in this pressure range, nor do they reflect a peculiar variation in the oxygen content as can be seen from Fig. 3.

DISCUSSION

In the present work, it is interesting to focus attention on the data analysis at oxygen pressures smaller than about 10^{-8}–10^{-6} atm, that is the pressure range where the minima of the conductivity isotherms are located and the isotherms reflect the behavior of the conductivity in equilibrium with the gas-phase oxygen. It should be noticed that at such small oxygen pressures, and at temperatures above 700°C, the oxygen content variations in the RP ferrites under study are much smaller compared to the total oxygen content, i.e., $\delta \ll 6 + x/2$, and that the conductivity isotherms in the vicinity of the minima are rather smooth. This behavior is indicative of the ion contribution σ_i in the total conductivity. The analysis of the pressure dependencies of the conductivity isotherms in the vicinity of the minima leads to the standard expression for a mixed oxygen ion-electron conductor

$$\sigma(T,\ pO_2) = \sigma_i(T) + \sigma_n^0(T)pO_2^{-1/4} + \sigma_p^0(T)pO_2^{+1/4}, \quad [1]$$

where σ_i(T) is pressure independent oxygen ion contribution, while σ_n^0(T) and σ_p^0(T) represent n- and p-type contributions, as extrapolated to $pO_2 = 1$ atm, respectively. The values of these parameters are obtained by fitting Eq. (1) to experimental isotherms (see Table 1). A comparison of the experimental and calculated total conductivity in $Sr_3Fe_2O_{6+\delta}$ is shown as an example in Fig. 5, where a satisfactory match of the calculated and measured results occurs. The obtained ion conductivity can be utilized in combination with the measured total conductivity in order to calculate the ion transference numbers t_i. These results are shown in Fig. 6 for oxides

TABLE 1
The Parameters for Total Conductivity in $Sr_3Fe_{2-x}Ti_xO_{6+\delta}$ at Different Temperatures

		Temperature (°C)					
x	Conductivity parameters	1000	950	900	850	800	750
0	σ_i	5.9×10^{-2}	3.3×10^{-2}	1.2×10^{-2}	5.8×10^{-3}	2.8×10^{-3}	1.9×10^{-3}
	σ_n^0	6.3×10^{-5}	2.5×10^{-5}	9.2×10^{-6}	2.9×10^{-6}	7.9×10^{-7}	1.9×10^{-7}
	σ_p^0	4.65	4.73	6.96	9.09	10.70	13.20
1.2	σ_I	$5.1 \times 10_{-3}$	3.4×10^{-3}	2.3×10^{-3}	1.6×10^{-3}	1.1×10^{-3}	7.3×10^{-3}
	σ_n^0	3.2×10^{-6}	1.6×10^{-6}	6.4×10^{-7}	2.3×10^{-7}	7.6×10^{-8}	2.1×10^{-8}
	σ_p^0	0.34	0.36	0.38	0.41	0.45	0.45

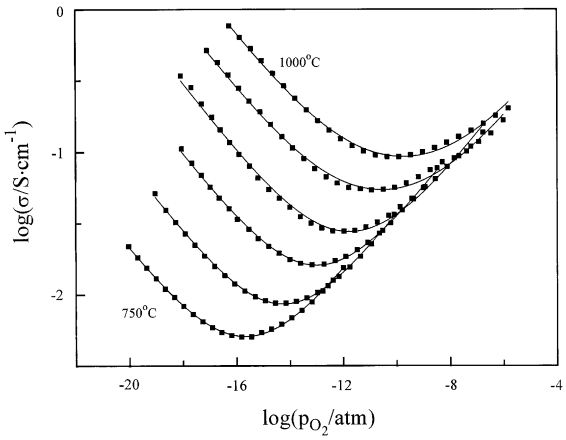

FIG. 5. Comparison of the experimental data and calculated results (solid lines) for a the conductivity in $Sr_3Fe_2O_{6+\delta}$.

with $x = 0$ and 1.2 and 900°C. It can be seen from a comparison of Figs. 4 and 6 that titanium substitution results in stronger suppression of the electron transport compared to the oxygen ion component. Therefore, the relative contribution of oxygen ions in the total conductivity becomes more significant with doping.

Electron Transport

The isothermal plots of the sum $\sigma_n + \sigma_p \equiv \sigma_{n,\,p}$ of partial n- and p- type electron contributions in the conductivity, obtained by the subtraction of the ion conductivity from the total conductivity, are shown in Fig. 7 for samples with $x = 0$ and 1.2. The slope of the conductivity isotherms approaches $-\frac{1}{4}$ and $+\frac{1}{4}$ at pO_2 values to the left and to the right of the minima. The negative slope is characteristic of electron-type carriers

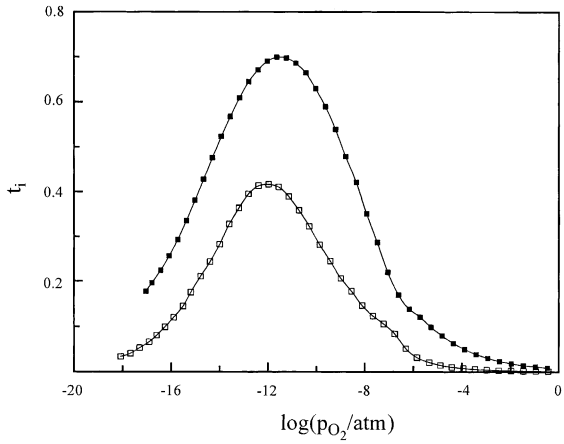

FIG. 6. The pressure variations in oxygen ion transference numbers at 900°C in $Sr_3Fe_2O_{6+\delta}$ (empty squares) and $Sr_3Fe_{0.8}Ti_{1.2}O_{6.6+\delta}$ (filled squares). Solid lines serve as a guide to the eye.

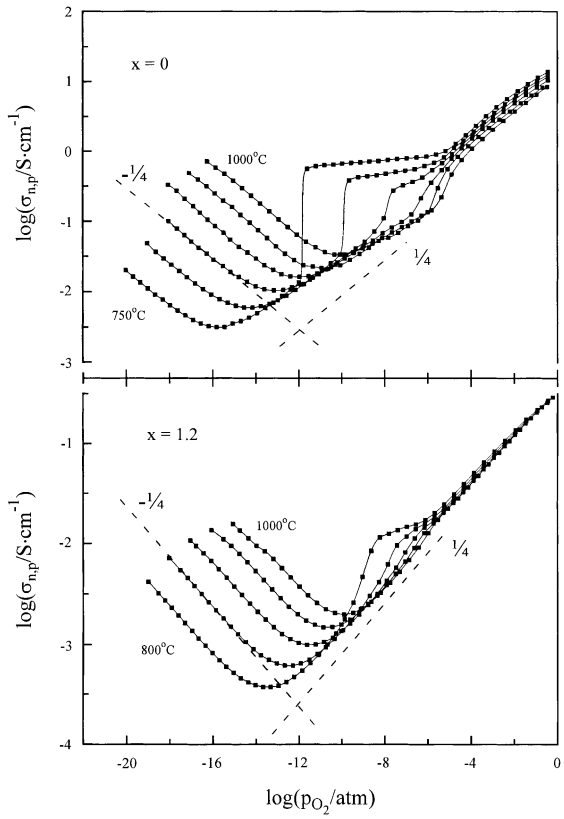

FIG. 7. The pressure dependencies at different temperatures of the electron conductivity in $Sr_3Fe_{2-x}Ti_xO_{6+\delta}$. Solid lines serve as a guide to an eye. Dashed lines show slopes of the isotherms left and right to the minima.

dominating the conductivity in the low pressure regime, while the positive slope is indicative of hole-type carriers becoming dominant when the pressure increases. Appearance of the conducting electrons, i.e., Fe^{2+} cations, in these materials may be explained by a loss of oxygen from the crystalline lattice of $Sr_3Fe^{2+}_{2\delta}Fe^{3+}_{2-x-2\delta}Ti^{4+}_xO_{6+x/2-\delta}$ in the low-pressure limit:

$$O^{2-} = \tfrac{1}{2}O_2 + 2e^-,$$
$$K_n = \frac{[e^-]^2 \cdot pO_2^{1/2}}{[O^{2-}]} = K_n^0 \exp\left(-\frac{\Delta H_n}{kT}\right). \qquad [2]$$

Here, K_n^0 is a constant and ΔH_n is the reaction enthalpy. From the above discussion, this quantity may also be regarded as the enthalpy of formation of oxygen vacancies in O(1) positions. Experimentally observed variations in the oxygen content δ near the minima of the conductivity are much smaller in comparison with the total amount of oxygen ions in the sample. Therefore, the oxygen content in the equilibrium constant K_n may be considered as nearly constant, i.e., $[O^{2-}] \approx 6 + x/2$. Hence, the power dependence $\sigma_n \propto [e^-] \propto pO_2^{-1/4}$ consistent with the experimental

TABLE 2
The Activation Energies (eV) for the Ion, p- and n- Type Contributions to Total Conductivity and for the Minimal Conductivity in $Sr_3Fe_{2-x}Ti_xO_{6+\delta}$

x	E_i	E_p	E_n	E_{p-n}
0	0.6	−0.4	2.70	1.15
1.2	0.6	−0.1	2.35	1.15

results follows from the equilibrium constant. The values of the activation energy for the n-type conductivity, E_n, in Table 2 are calculated from the Arrhenius plots for the electron conductivity at $pO_2 = 10^{-16}$ atm (Fig. 8a).

Development of the hole conductivity, i.e., the increase in amount of Fe^{4+} cations with oxygen pressure to the right of the minima in Fig. 7, reflects oxygen incorporation in the O(3) positions or $Sr_3Fe^{3+}_{2-x-2\delta}Fe^{4+}_{2\delta}Ti^{4+}_xO_{6+x/2+\delta}$

$$\tfrac{1}{2}O_2 = O^{2-} + 2h^+,$$
$$K_p = \frac{[h^+]^2[O^{2-}]}{pO_2^{1/2}} = K_p^0 \exp\left(-\frac{\Delta H_p}{kT}\right), \qquad [3]$$

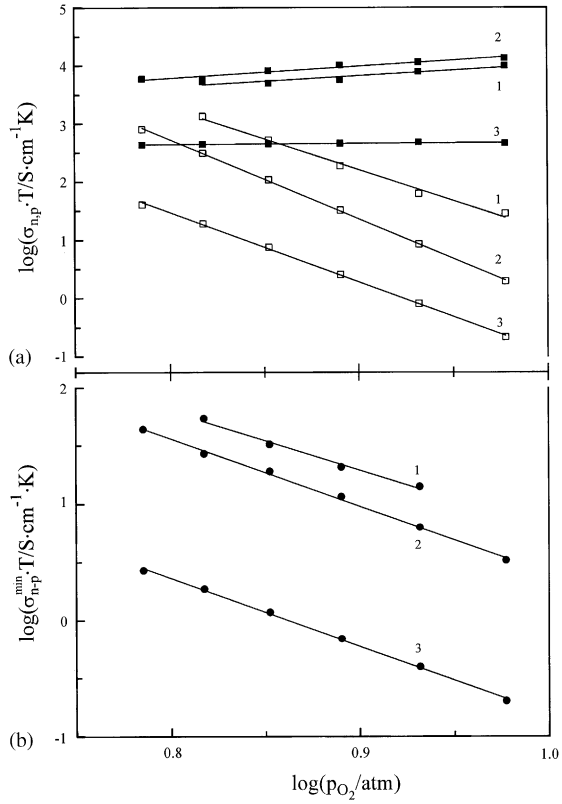

FIG. 8. (a) The Arrhenius plots for electron conductivity (empty squares) at $pO_2 = 10^{-16}$ atm and for hole conductivity (filled squares) at $pO_2 = 1$ atm in $Sr_2Fe_2O_5$ (1), $Sr_3Fe_2O_6$ (2) and $Sr_3Fe_{0.8}Ti_{1.2}O_{6.6}$ (3). (b) The Arrhenius plots for the minimal conductivity in $Sr_2Fe_2O_5$ (1), $Sr_3Fe_2O_6$ (2) and $Sr_3Fe_{0.8}Ti_{1.2}O_{6.6}$ (3). Solid lines show linear fitting to the data.

where K_p^0 is a constant and ΔH_p is the reaction enthalpy or, in other words, the enthalpy of oxygen at the O(3) positions. Again, given small variations in the total oxygen content $\delta \ll 6 + x/2$, the hole conductivity should increase with oxygen pressure as $\sigma_p \propto [h^+] \propto pO_2^{+1/4}$. Indeed, this pressure dependence agrees with the experimental results shown in Fig. 7. The p-type contribution $\sigma_p^0(T)$ at $pO_2 = 1$ atm, as obtained by fitting Eq. (1) to total conductivity, exhibits a weak decrease with the temperature increase, see Table 1. Thus the apparent activation energy for the hole conductivity E_p is a small negative quantity. Using the concentration of holes that follows from Eq. (3) for the equilibrium constant, and assuming temperature activated mobility of holes, the interrelation $E_p = \varepsilon_p + \Delta H_p/2$ can be obtained between the activation energy for the hole conductivity, the activation energy ε_p for the mobility of holes, and enthalpy ΔH_p. Thus, the observed small negative values for E_p show that oxygen incorporation reaction (3) is exothermic and suggests that $|\Delta H_p|/2$ is slightly larger than ε_p. The values for the p-type conductivity activation energy, E_p, in Table 2 are calculated from the Arrhenius plots for the hole conductivity at $pO_2 = 1$ atm, (Fig. 8a). Similar results (3) for electrons and holes in brownmillerite-like strontium ferrite $Sr_2Fe_2O_{5+\delta}$ are shown for comparison in Fig. 8a.

The high-temperature equilibrium of electrons and holes near the conductivity minima in Fig. 7 may be expressed as

$$0 = e^- + h^+ \qquad K_i = [h^+] \cdot [e^-] = K_i^0 \exp\left(-\frac{E_g}{kT}\right), \quad [4]$$

where E_g is the band gap and K_i^0 is a constant. The band gap may be estimated from the temperature dependence of the minimal conductivity, σ_{p-n}^{min}. Expressing concentrations of holes and electrons via respective partial contributions and mobilities, μ_p and μ_n, one can rearrange Eq. (4) in the form

$$K_i^0 \exp\left(-\frac{E_g}{kT}\right) = \left(\frac{\sigma_{p-n}^{min}}{2e(\mu_p\mu_n)^{1/2}}\right)^2. \qquad [5]$$

Presuming temperature-activated mobility for both holes and electrons

$$\mu_{p,\,n} = \frac{\mu_{p,n}^0}{T} \exp\left(-\frac{\varepsilon_{p,\,n}}{kT}\right), \qquad [6]$$

where ε_p and ε_n are the respective mobility activation energies, the value $E_g + \varepsilon_p + \varepsilon_n \equiv 2E_{p-n}$ can be found from the plots of $\log(\sigma_{p-n}^{min} \cdot T)$ versus reciprocal temperature as shown in Fig. 8b. Similar data for $Sr_2Fe_2O_{5+\delta}$ (3) are given for comparison. For the materials under study, the parameter E_{p-n} is found to be virtually invariable (see Table 2). The activation energy for migration of both

electrons and holes in the perovskite-like oxide $Sr_{1-x}La_xFeO_{3-\delta}$, where $x = 0.75$–1.0, is reported to be nearly zero (9). Assuming that the same holds true in the RP perovskite-related structure of $Sr_3Fe_{2-x}Ti_xO_{6+x/2+\delta}$, we find that $E_g \approx 2E_{p-n}$. The estimated values of the band gap when $x = 0$ and 1.2 are both equal to about 2.3 eV compared with 1.9 eV in $Sr_2Fe_2O_{5+\delta}$ (3). The band gap, weakly dependent on the titanium content, suggests that the titanium 3*d* states essentially do not participate in the formation of the gap, even when a fairly substantial amount of titanium replaces iron. Thus, the gap width in $Sr_3Fe_{2-x}Ti_xO_{6+x/2+\delta}$ is defined primarily by the interactions of the iron and oxygen ions. In other words, the top and bottom of the valence and conductance bands, respectively, are mainly formed from oxygen and iron states again, respectively. This conclusion is consistent with a considerable decrease of the electronic conductivity with iron content across the solid solution because with the decrease of iron content in the RP structure there is a decrease in the density of the near band gap states.

In the situation close to intrinsic electron–hole equilibrium, i.e., when oxygen non-stoichiometry parameter δ is close to zero, p-type conductivity is somewhat larger in $Sr_3Fe_2O_{6+\delta}$ than in $Sr_2Fe_2O_{5+\delta}$ and an order of magnitude greater than in $Sr_3Fe_{0.8}Ti_{1.2}O_{6.6+\delta}$. It is important to recognize that the crystalline structure of the RP oxide $Sr_3Fe_2O_{6+\delta}$ and of the brownmillerite-like ferrite $Sr_2Fe_2O_{5+\delta}$ are composed of FeO_2 sheets separated with layers of strontium oxide and iron–oxygen tetrahedra, respectively. Also, the number of such sheets per formula unit is two in $Sr_3Fe_2O_{6+\delta}$, while it is one in $Sr_2Fe_2O_{5+\delta}$. Therefore, the larger hole conductivity in $Sr_3Fe_2O_{6+\delta}$ compared to $Sr_2Fe_2O_{5+\delta}$ may be interpreted as evidence that hole conduction develops mainly in the iron-oxygen FeO_2 sheets, and a larger number of such "parallel conductors" results in a higher conductivity. In contrast, the electron contribution is appreciably smaller in $Sr_3Fe_2O_{6+\delta}$ than in $Sr_2Fe_2O_{5+\delta}$. This observation suggests that movement of electron-type carriers may occur not only in the FeO_2 sheets but involve also intersheet jumps via iron–oxygen tetrahedra in $Sr_2Fe_2O_{5+\delta}$, while such jumps would be strongly forbidden in $Sr_3Fe_2O_{6+\delta}$ where FeO_2 sheets are separated with insulating SrO layers. The considerable decrease of both p- and n-type contributions to conductivity in $Sr_3Fe_{0.8}Ti_{1.2}O_{6.6+\delta}$ compared to $Sr_3Fe_2O_{6+\delta}$ suggests that the titanium cations take little or no part in electron conduction.

Oxygen Ion Transport

The temperature dependencies of the obtained oxygen ion conductivity σ_i for $Sr_3Fe_2O_{6+\delta}$ and $Sr_3Fe_{0.8}Ti_{1.2}O_{6.6+\delta}$ are shown with Arrhenius coordinates in Fig. 9. These data show that filling of structural vacancies in the O(3) position, caused by partial replacement of iron for titanium, results in an appreciable decrease of the ion conductivity level in the entire temperature range studied. This observation gives direct evidence of the structural vacancies involved in the ion transfer. The apparent activation energy, E_i (see Table 1), for the ion conductivity in both the parent and titanium-doped ferrites below 800°C is equal to about 0.6 eV, a value typical for perovskite-like oxides. The activation energy, which is practically independent of the titanium content, implies that even rather large substitution of titanium for iron does not alter the ion migration mechanism in the low temperature extreme. At the same time, the conductivity values in the doped oxide are about 2.5 times smaller. A fast increase of the ion conductivity in $Sr_3Fe_2O_{6+\delta}$ can be seen in Fig. 9 as the temperature increases from about 800°C to 950°C. Simultaneously, the apparent activation energy increases with temperature up to about 2 eV. This value is far too large to be related solely with the ion transfer. Thus, heating facilitates another process that interferes with ion movement. This process appears to approach completion in $Sr_3Fe_2O_{6+\delta}$ at about 950°C because at yet higher temperatures the activation energy decreases substantially. Though less pronounced, the conductivity increase above 800°C is also seen distinctly in $Sr_3Fe_{0.8}Ti_{1.2}O_{6+\delta}$.

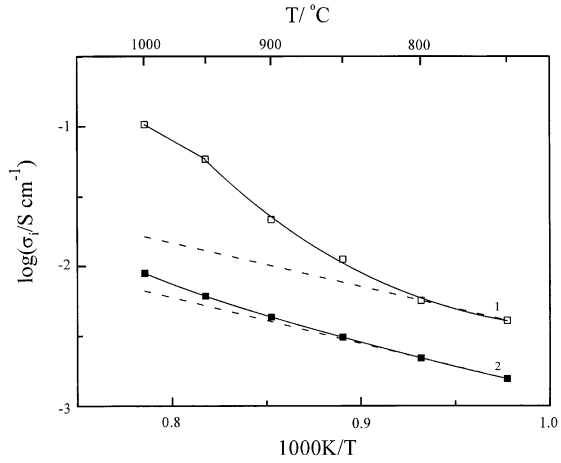

FIG. 9. The Arrhenius plots for the ion conductivity in $Sr_3Fe_2O_{6+\delta}$ (1) and $Sr_3Fe_{0.8}Ti_{1.2}O_{6.6+\delta}$ (2). Solid lines serve as a guide to the eye. Dashed lines show linear approximation to the data at low temperatures.

Let us first discuss the data for $Sr_3Fe_2O_{6+\delta}$ in the temperature range below 800°C. Based on structural considerations, where there is an ample amount of structural vacancies in O(3) position while O(1) positions are essentially filled, one may suggest that the "first" possible ion jump occurs from a O(1) position to a neighboring O(3) position as shown by arrow 1 in Fig. 10a

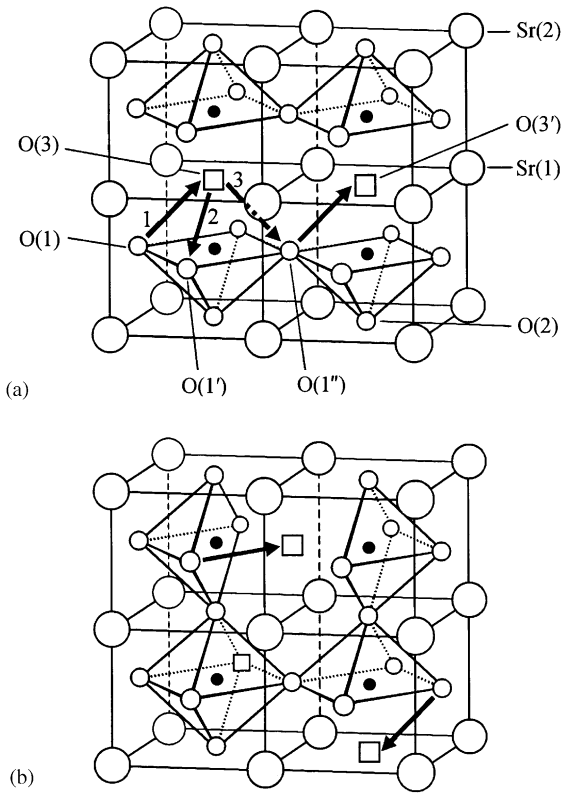

FIG. 10. The fragments of the crystalline lattice of the ordered (a) and disordered (b) RP ferrite. Arrows show possible ion jumps (see also comments in the text).

where the relevant fragment of the crystalline lattice is reproduced. This ion ↔ vacancy positional exchange is believed to occur in oxide perovskites with random vacancies. The next, direct jump of the ion to the nearby O(3′) structural vacancy would have a small probability because of the narrow spacing (~ 1.4 Å) for the oxygen ion ($r(O^{2-}) = 1.4$ Å (8)) to overcome between two strontium cations in the structure. Therefore, the backward (return) jump of the ion is most probable, but it does not contribute to the transfer. Notice, however, that during the time the ion is resting in the O(3) position, the vacancy left in the O(1) position may jump to the equivalent O(1′) position or even to the O(1″) position in the FeO_2 sheet, thus resulting in a probability for the ion to jump from the O(3) position to either O(1′) or O(1″) position as shown by arrows 2 and 3 in Fig. 10a, respectively. These jumps give a contribution to the transfer. In an ordinary migration mechanism over random vacancies, the jump trajectories for ions and vacancies are the same though oppositely directed. This is not always the case when structural vacancies are involved. For instance, the transfer of the oxygen ion from the O(1) position to the O(1″) position proceeds along the route O(1)→O(3)→O(1″) while the oxygen vacancy may move along O(3)→O(1)→O(1′)→O(1″). Certainly, the overall frequency prefactor in the oxygen ion diffusion coefficient must be smaller in the oxide with structural vacancies than in the perovskite with random vacancies. Therefore, the RP structure with ordered vacancies is indeed less favorable for ion conduction than is the perovskite structure. Nonetheless, the conductivity level is not negligibly small, which in combination with greater structural stability may be advantageous in applications. Based on the proposed mechanism the ion conductivity level should be proportional to the amount of structural vacancies per elementary unit. The amount of such vacancies in the high-temperature–low-pressure range, where $\delta \approx 0$, is equal to approximately unity in $Sr_3Fe_2O_{6+\delta}$ while it is nearly 0.4 in $Sr_3Fe_{0.8}O_{6.6+\delta}$. Hence, the 2.5 times larger ion conductivity in $Sr_3Fe_2O_{6+\delta}$ compared to $Sr_3Fe_{0.8}Ti_{1.2}O_{6.6+\delta}$ can be understood as reflecting the larger $(1/0.4 = 2.5)$ amount of the available structural vacancies.

The simultaneous increase in the conductivity and activation energy above 800°C may possibly be related to a partial disordering of the crystal lattice on heating. In the low oxygen pressure range where oxygen composition remains virtually invariable, such disordering may be envisioned as random partial redistribution of the structural vacancies over regular oxygen positions. The fragment of the disordered crystal lattice of the RP ferrite is shown in Fig. 10b. The randomization of the structural vacancies must result in some enlargement of the elementary unit parameters compared to those in the ordered lattice. In order to verify the disordering, two specimens of RP ferrite were annealed during 4 h at 1025°C in the 5% H_2:95% He atmosphere saturated with water vapor ($pO_2 \approx 10^{-13.5}$ atm). Then, one sample was quenched while the other one was allowed to cool slowly. The TG measurements confirmed an oxygen content close to 6 in both specimens. The X-ray patterns of both samples showed single-phase RP ferrite with the tetragonal unit cell parameters $a = 3.903(2)$ Å and $b = 20.074(5)$ Å for the quenched sample, both larger than the values $a = 3.896(2)$ Å and $b = 20.051(5)$ Å observed after slow cooling. This observation confirms the supposed disordering. The local structure of the disordered fragment in the RP ferrite is that of the perovskite with random vacancies. It is not surprising, therefore, that at temperatures above 950°C, where the disordering seems to be close to completion, the activation energy recovers to a smaller value while the ion conductivity achieves values characteristic for the disordered ferrite perovskite (10, 11). The titanium doping results in formation of rather rigid titanium–oxygen octahedra in the structure and irreversible filling of O(3) vacancies thus significantly decreasing the amount of oxygen vacancies that may be disordered by heating. Therefore, the conductivity increase in $Sr_3Fe_{0.8}Ti_{1.2}O_{6.6}$ on heating above 800°C is less pronounced.

CONCLUSIONS

We have studied the oxygen-deficient, titania-doped Ruddlesden–Popper (RP) ferrites $Sr_3Fe_{2-x}Ti_xO_{6+\delta}$ using X-ray powder diffraction, thermogravimetric analysis and conductivity measurements. Titanium replacement for iron is shown to occur over the entire range $0 \le x \le 2$. The doping does not change the basic tetragonal symmetry of the elementary unit in the solid solution. The changes in oxygen content and crystal lattice parameters reflect the replacement of iron cations for larger titanium cations where the latter exhibit a stable 4+ oxidation state and sixfold oxygen coordination. The parent all-iron ferrite and its titania-doped derivatives remain structurally stable and single phase at oxygen pressures down to 10^{-20} and 10^{-16} atm at 750°C and 1000°C, respectively. The pressure-dependent isotherms of the total conductivity for both $Sr_3Fe_2O_{6+\delta}$ and $Sr_3Fe_{0.8}Ti_{1.2}O_{6.6+\delta}$ were analyzed in the pressure range from 10^{-20} to 10^{-6} atm. It is shown that in this pressure range and temperatures above 750°C these oxides are mixed oxygen ion–electron conductors. The titanium doping favors an increase in the oxygen ion transference numbers. Electron-like carriers emerge in the RP structure as a result of appearance of oxygen vacancies, most probably in O(1) positions. The hole-like carriers appear in response to oxygen incorporation into structural vacancies in the O(3) position. Based on a comparison of the electron conductivity in the RP ferrite $Sr_3Fe_2O_{6+\delta}$ and in brownmillerite-like ferrite $Sr_2Fe_2O_{5+\delta}$, it is argued that both p- and n- type carriers move mainly in the iron–oxygen FeO_2 sheets in $Sr_3Fe_2O_{5+\delta}$. The electron–hole conductivity level in the RP ferrites with $\delta \approx 0$, both parent and titania-doped, is governed by the forbidden gap of about 2.3 eV while the activation energy for mobility of both holes and electrons is small. The oxygen ion partial contribution is found from the analysis of the pressure dependencies of the total conductivity. It is shown that movement of oxygen ions in the ferrite occurs in the iron–oxygen sheets via indirect jumps involving structural vacancies in the O(3) position at temperatures below 800°C. The introduction of titanium results in a decrease of the ion conductivity, which can be explained by a partial filling of the structural vacancies and blocking of the indirect jumps. An increase in temperature is shown to cause disordering of the structural vacancies which in turn increases the ion conductivity to about 0.06 S/cm in $Sr_3Fe_2O_{6+\delta}$ at 950–1000°C.

ACKNOWLEDGMENTS

We acknowledge partial support of this work by the Russian Foundation for Basic Research (Grant 01-03-96519) and by sixth competition of the RAS young scientists (Grant 192). One of us (K.R.P.) is grateful to the EMSI program of the National Science Foundation and the US Department of Energy Office of Science (CHE-9810378) at the Northwestern University Institute for Environmental Catalysis.

REFERENCES

1. J. E. ten Elshof, H. J. M. Bouwmeester, and H. Verweij, *Solid State Ionics* **81,** 97–109 (1995).
2. M. Schwartz, J. White, and A. Sammels, International Patent Application PCT WO 97/41060, 1997.
3. V. L. Kozhevnikov, I. A.Leonidov, M. V. Patrakeev, E. B. Mitberg, and K. R. Poeppelmeier, *J. Solid State Chem.* **158,** 320–326 (2000), doi:10.1006/jssc.2001.9120.
4. F. Prado and A. Manthiram, *J. Solid State Chem.* **158,** 307–314 (2001), doi:10.1006/jssc.2001.9111.
5. S. E. Dann, M. T. Weller, and D. B. Currie, *J. Solid State Chem.* **97,** 179–185 (1992).
6. R. J. Nadalin and W. B. Brozda, *Anal. Chim. Acta* **28,** 282–293 (1963).
7. M. V. Patrakeev, E. B. Mitberg, I. A. Leonidov, and V. L. Kozhevnikov, *Solid State Ionics* **139,** 325–330 (2001).
8. R. D. Shannon, *Acta Crystallogr.* **32,** 751 (1976).
9. J. Mizusaki, T. Sasamo, W. R. Cannon, and H. K. Bowen, *J. Amer. Ceram. Soc.* **66,** 247–252 (1983).
10. T. Ishigaki, S. Yamauchi, K. Kishio, J. Mizusaki, and K. Fueki, *J. Solid State Chem.* **73,** 179–187 (1988).
11. M. C. Kim, S. J. Park, H. Haneda, J. Tanaka, T. Mitsuhasi, and S. Shirasaki, *J. Mater. Sci. Lett.* **9,** 102–104 (1990).